

From global synaptic activity to neural networks topology: a dynamical inverse problem

Raffaella Burioni,^{1,2} Mario Casartelli,^{1,2} Matteo di Volo,^{1,3,2} Roberto Livi,^{4,5,6,3} and Alessandro Vezzani^{7,1}

¹*Dipartimento di Fisica e Scienza della Terra, Università di Parma, via G.P. Usberti, 7/A - 43124, Parma, Italy*

²*INFN, Gruppo Collegato di Parma, via G.P. Usberti, 7/A - 43124, Parma, Italy*

³*Centro Interdipartimentale per lo Studio delle Dinamiche Complesse, via Sansone, 1 - 50019 Sesto Fiorentino, Italy*

⁴*Dipartimento di Fisica, Università di Firenze, via Sansone, 1 - 50019 Sesto Fiorentino, Italy*

⁵*Istituto dei Sistemi Complessi, CNR, via Madonna del Piano 10 - 50019 Sesto Fiorentino, Italy*

⁶*INFN Sez. Firenze, via Sansone, 1 - 50019 Sesto Fiorentino, Italy*

⁷*S3, CNR Istituto di Nanoscienze, Via Campi, 213A - 41125 Modena, Italy*

Making use of heterogeneous mean-field equations for a leaky-integrate-and-fire neural dynamics with short term plasticity on random networks, we formulate and solve the inverse problem of reconstructing the in-degree distribution from the knowledge of the global activity field. This approach also provides an effective description of very large systems, whose main microscopic and collective dynamical features can be reproduced and studied analytically. The generality of the method goes beyond the application to neural dynamics and can be useful in experimental studies.

PACS numbers: 87.19.lj, 05.45.Xt, 89.75.Hc, 02.30.Zz

Models of dynamical rules on networks are of interest for many different fields, ranging from physics to biology and social sciences. In particular, the influence of the network topology onto the dynamics has recently attracted the interest of theoreticians and applied scientists [1–6]. Research in this field has focused in two main directions. The *direct problem* aims at predicting the dynamical properties of a network from its topological parameters, searching for the optimal engineered topologies for a given task [7]. The *inverse problem* is addressed to the reconstruction of the network features from measurements of time series produced by the dynamics [8–10]. The latter approach is particularly interesting when the direct investigation of the network is impossible or very hard to be performed. Neural networks are typical examples of such a situation. Measurements of the signals emerging from neural time evolution are often records of the global synaptic activity from large regions of the cerebral cortex – a kind of observable that is expected to be measured much more easily and safely, than signals coming from single neuron activities [11, 12]. Inferring the topological properties of the network from such global signals is still an open and central problem in neurophysiology. In this letter we investigate the possibility of answering the following question: given a global, i.e. average, synaptic-activity field, which kind of network topology has generated it?

As an example of neural network dynamics we focus on a system of leaky integrate-and-fire (LIF) excitatory neurons, interacting via a synaptic current regulated by the short-term plasticity mechanism [13, 14]. This model is able to reproduce synchronization patterns observed in *in vitro* experiments [16–18]. As a model for the underlying topology we consider randomly uncorrelated diluted networks made of N nodes. In general N is considered quite a large number, as well as the number of connections between pairs of neurons. This suggests that the right framework for understanding large-population neu-

ral networks should be a mean-field approach, where the thermodynamic limit, $N \rightarrow \infty$ is expected to provide the basic ingredients for an analytic treatment. On the other hand, the way such a thermodynamic limit is performed may wipe out any relation with the topological features that are responsible, for finite N , of relevant dynamical properties of the network dynamics. In Erdős–Renyi directed networks, where each neuron is randomly and uniformly connected to a finite fraction of the other neurons (*massive connectivity*), the fluctuations of the degree determine a rich dynamical behavior. This is characterized by quasi-synchronous events (QSE): a large fraction of neurons fire in a short time interval of a few milliseconds (ms), separated by uncorrelated firing activity lasting over some tens of ms. However, such a behavior is lost in the thermodynamic limit, as the fluctuations of the connectivity vanish and the “mean-field-like” dynamics reduces to a state of fully synchronized neurons (e.g., see [19]). In order to maintain in the large N limit the QSE phenomenology, we can rather consider the sequence of random graphs that keep the same specific in-degree distribution $P(\bar{k})$ ($\bar{k}_i = k_i/N$ is the fraction of incoming neurons connected to neuron i), for any finite N , similarly to the configuration models [20]. This way of performing the thermodynamic limit preserves the dynamical regime of QSE and the difference between synchronous and non-synchronous neurons according to their specific in-degree k . By introducing explicitly this $N \rightarrow \infty$ limit in the differential equations of our dynamical model, we obtain a *heterogeneous mean-field* (HMF) description, similar to the one recently introduced in the context of epidemiological spreading on networks [2, 3]. These mean-field like equations can be studied analytically. In particular, we find that a sufficiently narrow distributions of $P(\bar{k})$ is necessary to observe the quasi-synchronous dynamical phase, while for broad distributions of \bar{k} synchronous activity is suppressed.

More importantly, these mean-field equations allow us

to design an inverse problem approach, that can be formulated in terms of an integral Fredholm equation of the first kind in $P(\tilde{k})$ [15]. By solving this equation, we are able to determine with good accuracy the $P(\tilde{k})$ of the network from the dynamical signal of the average synaptic-activity field. We test this method for very different uncorrelated network topologies, where $P(k)$ ranges from a Gaussian with one or several peaks, to power-law distributions, showing its effectiveness even for finite size networks. We want to point out that the overall procedure applies to a wide class of neural network dynamics of the type

$$\dot{\mathbf{w}}_i = \mathbf{F}\left(\mathbf{w}_i, \frac{g}{N} \sum_{j \neq i} \epsilon_{ji} G(\mathbf{w}_j)\right), \quad (1)$$

where the vector \mathbf{w}_i represents the state of neuron i , $\mathbf{F}(\mathbf{w}_i, 0)$ is the single neuron dynamics, g is the coupling strength, $G(\mathbf{w}_j)$ is a suitable coupling function between neurons and $\epsilon_{j,i}$ is the adjacency matrix of the directed uncorrelated network, whose entries are equal to 1 if neuron j fires to neuron i and 0 otherwise.

Here we illustrate the procedure for a network of N excitatory LIF neurons interacting via a synaptic current, regulated by short-term-plasticity with equivalent synapses [16]. In this case $\mathbf{w}_i = (v_i, x_i, y_i, z_i)$ where v_i is the rescaled membrane potential and x_i, y_i , and z_i represent the fractions of synaptic transmitters in the recovered, active, and inactive state, respectively ($x_i + y_i + z_i = 1$). Eq. (1) specializes to:

$$\dot{v}_i = a - v_i + \frac{g}{N} \sum_{j \neq i} \epsilon_{ji} y_j \quad (2)$$

$$\dot{y}_i = -\frac{y_i}{\tau_{\text{in}}} + u x_i S_i \quad (3)$$

$$\dot{z}_i = \frac{y_i}{\tau_{\text{in}}} - \frac{z_i}{\tau_r}. \quad (4)$$

Whenever the potential $v_i(t)$ reaches the threshold value $v_{\text{th}} = 1$, it is reset to $v_r = 0$, and a spike is sent towards the postsynaptic neurons. The spike is assumed to be a δ -like function of time. Accordingly, the spike-train $S_j(t)$ produced by neuron j , is defined as $S_j(t) = \sum_m \delta(t - t_j(m))$, where $t_j(m)$ is the time when neuron j fires its m -th spike. The transmission of the field $S_j(t)$ is mediated by the synapse dynamics. Only the active transmitters react to the incoming spikes $S_i(t)$: the parameter u tunes their effectiveness, τ_{in} is the characteristic decay time of the postsynaptic current, while τ_r is the recovery time from synaptic depression. We assume that all parameters appearing in the above equations are independent of the neuron indices, and that each neuron is connected to a macroscopic number, $\mathcal{O}(N)$, of pre-synaptic neurons: this is the reason why the interaction term is divided by the factor N . In all data hereafter reported we have used phenomenological values of the rescaled parameters: $\tau_{\text{in}} = 0.2$, $\tau_r = 133\tau_{\text{in}}$, $a = 1.3$, $g = 30$ and $u = 0.5$ [19]. Numerical simulations

can be performed effectively by transforming the set of differential equations (2)–(4) into an event-driven map [19, 21, 22]. On Erdős–Renyi random graphs, where each link is accepted with probability p , so that $\langle k \rangle = pN$, the dynamics has been analyzed in detail [19]. Neurons separate spontaneously into two different families: the *locked* and the *unlocked* ones. The locked neurons determine quasi-synchronous events (QSE) and exhibit a periodic dynamics. The unlocked ones participate to the uncorrelated firing activity and exhibit a sort of irregular evolution. Neurons belong to one of the two families according to their in-degree k_i . In this topology, the thermodynamic limit can be simply worked out. Unfortunately, this misses all the interesting features emerging from the model at finite N . Actually, for any finite value of N the in-degree distribution is centered around $\langle k \rangle$, with a variance $\sigma \sim N^{\frac{1}{2}}$. The effect of disorder is quantified by the ratio $\sigma/\langle k \rangle$, that vanishes for $N \rightarrow \infty$. Hence the thermodynamic limit reproduces the naive mean-field like dynamics of a fully coupled network, with rescaled coupling $g \rightarrow pg$, that is known to eventually converge to a periodic fully synchronous state [19].

On the other hand, uncorrelated random graphs can be defined by different protocols, that keep track of the in-degree inhomogeneity also in the thermodynamic limit. In our construction we fix the normalized in-degree probability distribution $P(\tilde{k})$, so that $\sigma/\langle k \rangle$ is kept constant for any N [20]. Accordingly, $P(\tilde{k})$ is a normalized distribution defined in the interval $\tilde{k} \in [0, 1]$ (while the number of inputs $k \in [0, N]$). In particular, if $P(\tilde{k})$ is a truncated Gaussian distribution, the dynamics reproduces the scenario observed in [19] for an Erdős–Renyi random graph. In fact, also in this case neurons are dynamically distinguished into two families, depending on their in-degree. In particular, neurons with \tilde{k} in between two *critical values*, \tilde{k}_{c1} and $\tilde{k}_{c2} \approx \langle \tilde{k} \rangle$, are locked and determine the QSE: they fire with almost the same period, but exhibit different (\tilde{k} -dependent) phases. All the other neurons are unlocked and fire in between QSE displaying an intermittent behavior. Notice that the range $0 < \tilde{k} < \tilde{k}_{c1}$ corresponds to the left tail of the truncated gaussian distribution; accordingly, the large majority of unlocked neurons is found in the range $\tilde{k}_{c2} < \tilde{k} < 1$ (for details see Supplementary Materials [23]). In order to characterize the dynamics for increasing values of N we consider for each neuron its inter-spike-interval (ISI), i.e. the lapse of time in between consecutive firing events. In Fig.1 we show $\overline{ISI}(\tilde{k})$, i.e. the time-average of ISI vs \tilde{k} . One can clearly observe the plateau of locked neurons and the crossover to unlocked neurons at the critical values \tilde{k}_{c1} and \tilde{k}_{c2} . Remarkably, networks of different sizes ($N = 500, 5000$ and 20000) feature the same $\overline{ISI}(\tilde{k})$ for locked neurons, and almost the the same values of \tilde{k}_{c1} and \tilde{k}_{c2} . There is not a sharp transition from locked to unlocked neurons, because for finite N the behavior of each single neuron depends not only on its \tilde{k} , but also on the neurons sending it their inputs. Nevertheless, in the inset the crossover

appears to be sharper and sharper for increasing N , as expected for true critical points. Furthermore, the fluctuations of $\overline{ISI}(\tilde{k})$ over different realizations, by $P(\tilde{k})$, of three networks of different size exhibit a peak around \tilde{k}_{c1} and \tilde{k}_{c2} , while they decrease with N as $\sim N^{-1/2}$ (data not shown). Thus, the qualitative and quantitative features of the QSE at finite sizes are expected to persist in the thermodynamic limit, where fluctuations vanish and the dynamics of each neuron depends only on its in-degree.

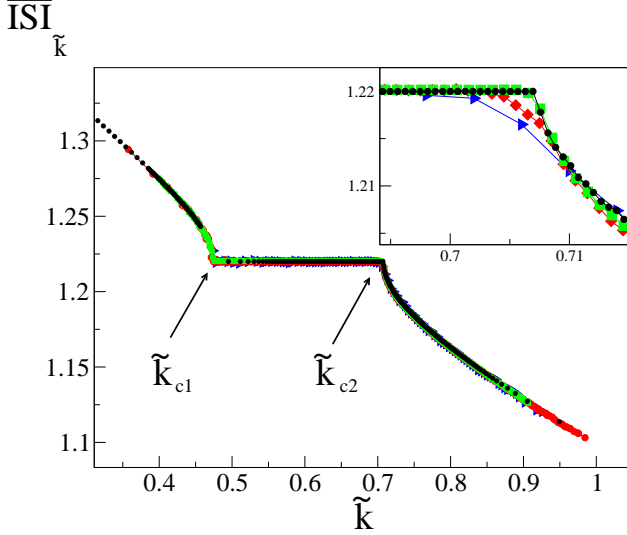


FIG. 1: (Color online) $\overline{ISI}_{\tilde{k}}$ vs \tilde{k} from a truncated Gaussian distribution $P(\tilde{k})$ with $\langle \tilde{k} \rangle = 0.7$ and $\sigma = 0.077$ and for three networks with $N = 500$ (light grey triangles, blue on line), $N = 5000$ (grey diamonds, red on line), $N = 20000$ (very light grey squares, green on line). For each size we have averaged the values of $\overline{ISI}_{\tilde{k}}$ over 8 different realizations of the random network. We have also performed a suitable binning over the values of \tilde{k} , thus yielding the numerical estimates of the critical values $\tilde{k}_{c1} \approx 0.49$ and $\tilde{k}_{c2} \approx 0.70$. In the inset we show a blow-up of the crossover region close to $\langle \tilde{k} \rangle = 0.7$. The black dots are the result of the simulation of the mean field dynamics (see Eq.s (6) – (8)) with $M = 307$.

We can obtain the Heterogeneous Mean-Field (HMF) version of Eq.s (2)–(4) by combining this thermodynamic limit procedure with a consistency relation. The input field received by neuron i is $Y_i = 1/N \sum_j \epsilon_{ij} y_j(t) = 1/N \sum_{j \in I(i)} y_j$, where $I(i)$ is the set of k_i neurons transmitting to neuron i . For very large values of N the average field received by neuron i , i.e. $1/k_i \sum_{j \in I(i)} y_j$, can be approximated with $1/N \sum_j y_j$, where the second sum runs over all neurons in the network (*mean-field hypothesis*). Accordingly, we have $Y_i \approx k_i/N \sum_j y_j$: as a consequence in the thermodynamic limit the dynamics of each neuron depends only on its specific in-degree. In the thermodynamic limit \tilde{k}_i becomes a continuous variable, independent of the label i and taking values in the inter-

val $[0,1]$. Finally, we can replace Y_i with $\tilde{k}Y(t)$, where

$$Y(t) = \int_0^1 P(\tilde{k}) y_{\tilde{k}}(t) d\tilde{k} \quad (5)$$

The HMF equations, then, read

$$\dot{v}_{\tilde{k}}(t) = a - v_{\tilde{k}}(t) + g\tilde{k}Y(t) \quad (6)$$

$$\dot{y}_{\tilde{k}}(t) = -\frac{y_{\tilde{k}}(t)}{\tau_{in}} + u(1 - y_{\tilde{k}}(t) - z_{\tilde{k}}(t))S_{\tilde{k}}(t) \quad (7)$$

$$\dot{z}_{\tilde{k}}(t) = \frac{y_{\tilde{k}}(t)}{\tau_{in}} - \frac{z_{\tilde{k}}(t)}{\tau_r}. \quad (8)$$

Despite this set of equations cannot be solved explicitly, they provide a great numerical advantage with respect to direct simulations of large systems. Actually, the basic features of the dynamics of such systems can be effectively reproduced (modulo finite-size corrections) by exploiting a suitable sampling of $P(\tilde{k})$. For instance, one can sample the continuous variable $\tilde{k} \in [0, 1]$ into M discrete values \tilde{k}_i in such a way that $\int_{\tilde{k}_i}^{\tilde{k}_{i+1}} P(\tilde{k}) d\tilde{k}$ is kept fixed (importance sampling). In Fig. 1 (black dots) we compare $\overline{ISI}(\tilde{k})$, obtained from the HMF equations for $M = 307$, with the same quantity computed by direct simulations of networks up to size $N = 2 \times 10^4$. The agreement is remarkable. Equations (6)–(8) allow us to perform efficiently also the stability analysis in terms of maps worked out by Tsodyks et al. [24] on a different model. This analysis, shown in the Supplementary Materials [23], points out the presence of a phase shift between locked neurons with different \tilde{k} . It indicates also that the unlocked neurons dynamics is characterized by intermittency, thus confirming that the weak chaotic nature of the dynamics is essentially due to the unlocked component. Finally, it allows to estimate the critical values \tilde{k}_c of the in-degree separating the locked and the unlocked families of neurons. Still in the perspective of the *direct problem*, the HMF equations provide further insight on how the network topology influences the dynamical behavior. We have found that, in general, the fraction of locked neurons increases as $P(\tilde{k})$ becomes sharper and sharper, while synchronization is eventually lost for broader distributions. In Fig. 2 we report the fraction of locked neurons, f_l , as a function of the variance σ , for different kinds of $P(\tilde{k})$ (single or double-peaked Gaussian, power-law) in the HMF equations. In all of these cases there is a critical value of σ above which f_l vanishes, i.e. QSE disappears. The generality of this scenario points out the importance of the relation between $P(k)$ and the average synaptic field $Y(t)$.

Finally, the HMF approach allows to implement the inverse problem, providing the distribution $P(\tilde{k})$ from the knowledge of $Y(t)$. In fact, if the global synaptic activity field $Y(t)$ is known, each class of neurons of in-degree \tilde{k}

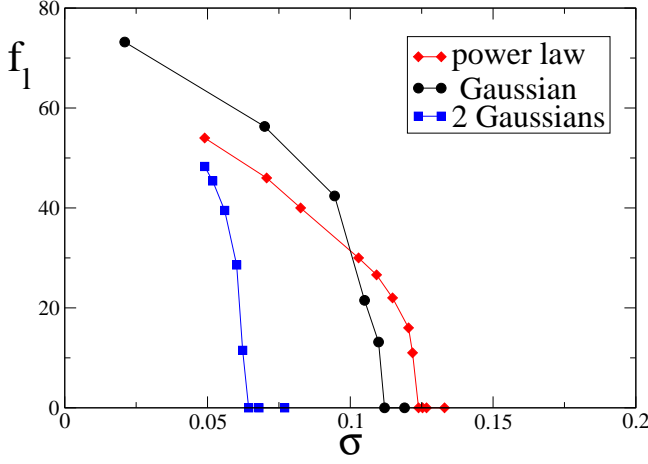


FIG. 2: (Color on line) The fraction of locked neurons, f_l , as a function of the variance σ of the distributions: truncated Gaussian with $\langle \tilde{k} \rangle = 0.7$ (black dots, black on line); truncated superposition of two Gaussians (both with variance 0.03), one centered at $\tilde{k}_1 = 0.5$ and the other one at a varying value \tilde{k}_2 , that determines the overall variance σ (grey squares, blue on line); truncated power-law distribution $P(\tilde{k}) \sim \theta(\tilde{k} - \tilde{k}_{\min})\tilde{k}^{-\alpha}$ with $\tilde{k}_{\min} = 0.1$ (light grey diamonds, red on line). In the last case the value of the variance is changed by varying the power α . Lines have been drawn just to guide the eyes.

evolves according to the equations:

$$\dot{v}_{\tilde{k}}(t) = a - v_{\tilde{k}}(t) + g\tilde{k}Y(t) \quad (9)$$

$$\dot{y}_{\tilde{k}}(t) = -\frac{y_{\tilde{k}}(t)}{\tau_{\text{in}}} + u(1 - y_{\tilde{k}}(t) - z_{\tilde{k}}(t))\tilde{S}_{\tilde{k}}(t) \quad (10)$$

$$\dot{z}_{\tilde{k}}(t) = \frac{y_{\tilde{k}}(t)}{\tau_{\text{in}}} - \frac{z_{\tilde{k}}(t)}{\tau_r} \quad (11)$$

Notice that each variable $v(t)$, $y(t)$, $z(t)$ can take different values from the variables generating the field $Y(t)$, i.e. $v(t)$, $y(t)$, $z(t)$, as starting from different initial conditions. However, the self consistent relation for the global field $Y(t)$ implies:

$$Y(t) = \int_0^1 P(\tilde{k})y_{\tilde{k}}(t)d\tilde{k} \quad (12)$$

If $Y(t)$ and $y_{\tilde{k}}(t)$ are known, this is a Fredholm equation of the first kind in $P(\tilde{k})$ [15]. In the general case of Eq. (1), calling $E(t)$ the global measured external field, the evolution equations corresponding to Eq.s (9)–(11) read

$$\dot{\mathbf{w}}_{\tilde{k}} = \mathbf{F}(\mathbf{w}_{\tilde{k}}, g\tilde{k}E(t)) \quad (13)$$

and the Fredholm equation for the inverse problem is

$$E(t) = \int_0^1 P(\tilde{k})G(\mathbf{w}_{\tilde{k}}(t))d\tilde{k} \quad (14)$$

In the case of our LIF model, as soon as a locked component exists, Eq. (12) can be solved by a functional

Montecarlo minimization procedure applied to a sampled $P(\tilde{k})$. At variance with the *direct problem*, $P(\tilde{k})$ is the unknown function and, accordingly, we have to adopt a uniform sampling of the support of \tilde{k} . A sufficiently fine sampling has to be used for a confident reconstruction of $P(\tilde{k})$ (See Supplementary Materials for details [23]).

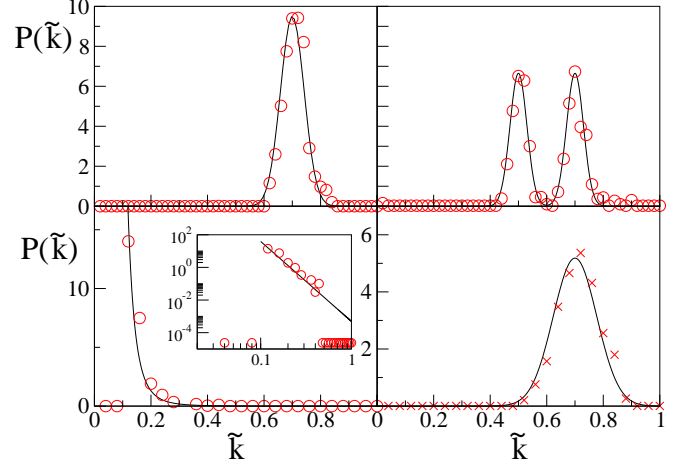


FIG. 3: The upper and lower-left panels show three distributions $P(\tilde{k})$ of the kind considered in Fig. 2 (black continuous curves) for the HMF equations (5)–(8) and their reconstructions (circles) by the inverse method based on equations (9)–(12). The parameters of the three distributions are $\sigma = 0.043$, $\tilde{k}_2 = 0.7$ and $\alpha = 4.9$. In the lower-right panel we show the reconstruction (crosses) of $P(\tilde{k})$ (black continuous line) by the average field $Y(t)$ generated by the dynamics of a *finite size* network with $N = 500$.

To check our inverse method, we choose a distribution $P(\tilde{k})$, evolve the system and extract the global synaptic field $Y(t)$. We then verify if the procedure reconstructs correctly the original distribution $P(\tilde{k})$. In the first three panels of Fig. 3 we show examples in which $Y(t)$ has been obtained from the simulation of the HMF with different $P(\tilde{k})$ (Gaussian, double peak Gaussian and power law). We can see that the method determines confidently the original distribution $P(\tilde{k})$. Notice that the method fails as soon as the locked component disappears. Remarkably, the method can recognize the discontinuity of the distribution in $\tilde{k} = \tilde{k}_{\min}$ and the value of the exponent of the power law $\alpha = 4.9$. Finally, in the last panel of Fig. 3, we show the result of the inverse problem for the distribution $P(\tilde{k})$ obtained from a global signal generated by a finite size realization with $N = 500$. The significant agreement indicates that the HMF and its inverse problem are able to infer the in-degree probability distribution $P(\tilde{k})$ even for a realistic finite size network. This last result is of particular importance, as it could unveil new perspectives for experimental data analysis from finite size samples. Even if our results have been illustrated in the case of uncorrelated networks, an interesting further

development would be to extend our approach by taking into account networks with degree correlations [3], that are known to characterize real structures.

I. SUPPLEMENTARY MATERIALS

A. Dynamics and stability analysis

Dynamical equations (2)–(4) on an Erdős–Rényi random network with dilution factor p were analyzed in detail in [18]. For large values of the network size, N , the in-degree distribution $P(\tilde{k})$ can be approximated by a Gaussian with average $\langle \tilde{k} \rangle = p$ and variance $\sigma = [p(1-p)/N]^{\frac{1}{2}}$, the latter vanishing in the thermodynamic limit.

Conversely, the thermodynamic limit yielding the HMF model described in the main text is performed fixing a given in-degree distribution $P(\tilde{k})$, where both the average and the variance are independent of N . As an example, in Fig.4 we show the raster plot of the dynamics of a random network containing $N = 500$ neurons, whose in-degree distribution $P(\tilde{k})$ is a Gaussian with average $\langle \tilde{k} \rangle = 0.7$ and variance $\sigma = 0.077$. The dynamics is very similar to the one obtained for an Erdős–Rényi random network (although in that case $\sigma \approx 0.02$).

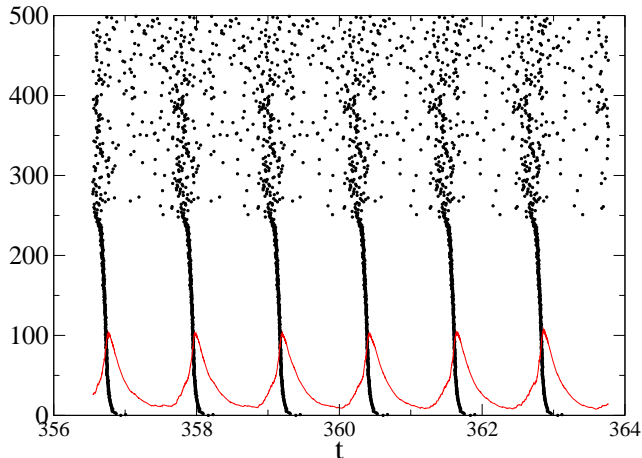


FIG. 4: (Color online) Raster plot representation of the dynamics of a network of $N = 500$ neurons with a Gaussian $P(\tilde{k})$ ($\langle \tilde{k} \rangle = 0.7$, $\sigma = 0.077$). Black dots signal single firing events of neurons at time t . Neurons are naturally ordered along the vertical axis according to the values of their in-degree. The global field $Y(t)$ (red line) is superposed to the raster plot for comparison (its actual values are multiplied by the factor 10^3 , to make it visible on the vertical scale).

The global field $Y(t) = \sum_i y_i(t)/N$ shows, apart from small fluctuations, a periodic dynamics peaked at the QSE. The neurons split into two families, locked and un-

locked ones, depending on their dynamics. Locked neurons feature a fixed firing time delay with respect to the peak of the field $Y(t)$. Furthermore, the firing time of locked neurons with respect to $Y(t)$ shows a phase shift depending on their in-degree. Unlocked neurons follow a complex dynamics with irregular firing times and typically they have an in-degree $\tilde{k} > \langle \tilde{k} \rangle$.

From the HMF equations (6)–(8), once the global field $Y(t)$ is known, the dynamics of each class of neurons with in-degree \tilde{k} can be determined by a straightforward integration. Moreover, one can perform the stability analysis that Tsodyks et al. applied to a similar model [24]. As an example, we have considered the system studied in Fig.4. The global field $Y(t)$ of the HMF dynamics has been obtained using the importance sampling for the distribution $P(\tilde{k})$. We have fitted $Y(t)$ with an analytic function of time $Y_f(t)$, continuous and periodic in time, with period T . Accordingly, Eq. (6) can be approximated by

$$\dot{v}_{\tilde{k}}(t) = a - v_{\tilde{k}}(t) + g\tilde{k}Y_f(t). \quad (15)$$

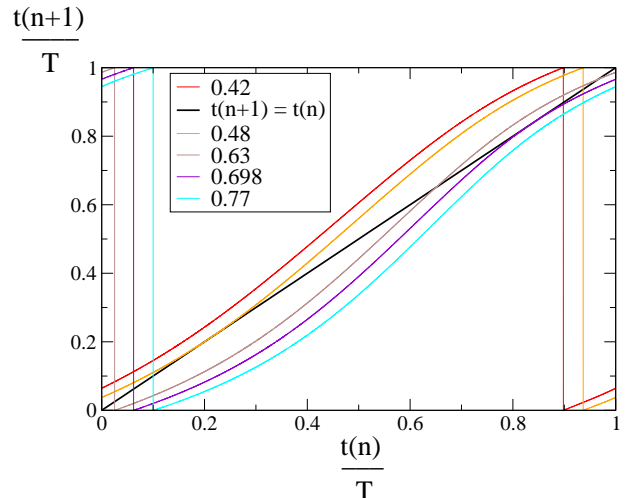


FIG. 5: (Color online) The return map $R_{\tilde{k}}$ (Eq. (16)) of the rescaled variables $t_{\tilde{k}}(n)/T$ for different values of \tilde{k} , corresponding to lines of different colors, according to the legend in the inset: the black line is the bisector of the square.

Notice that, by construction, the field $Y_f(t)$ features peaks at times $t = nT$, where n is an integer. In this way we can represent Eq. (15) as a Poincaré map. In practice, we integrate Eq.(15) and determine the sequence of the (absolute value of the) firing time-delay, $t_{\tilde{k}}(n)$, of neurons with in-degree \tilde{k} with respect to the reference time nT . The return map $R_{\tilde{k}}$ of this quantity reads

$$t_{\tilde{k}}(n+1) = R_{\tilde{k}}t_{\tilde{k}}(n). \quad (16)$$

In Fig. 5 we plot the return map of the rescaled firing time-delay $t_{\tilde{k}}(n)/T$ for different values of \tilde{k} . We observe

that in-degrees \tilde{k} corresponding to locked neurons (e.g., the brown curve) have two fixed points t_k^s and t_k^u , the first one is stable and the second unstable. Clearly, the dynamics converges to the stable fixed point displaying a periodic behavior. In particular, the firing times of neurons \tilde{k} are phase shifted of a quantity t_k^s with respect to the peaks of the fitted global field. The orange and violet curves correspond to the dynamics at the critical in-degrees \tilde{k}_{c1} and \tilde{k}_{c2} where the fixed points disappear (see Fig.(2) in the main text). The presence of such fixed points influences also the behavior of the unlocked component (e.g., the red and light blue curves). In particular, the nearer \tilde{k} is to \tilde{k}_{c1} or to \tilde{k}_{c2} , the closer is the return map to the bisector of the square, giving rise to a dynamics spending longer and longer times in an almost periodic firing. Afterwards, unlocked neurons depart from this almost periodic regime, thus following an intermittent chaotic behavior. As a byproduct, this dynamical analysis allows to estimate the values of the critical in-degrees. For the system of Fig.4, $\tilde{k}_{c1} = 0.48$ and $\tilde{k}_{c2} = 0.698$, in very good agreement with the numerical simulations.

B. Montecarlo approach to the inverse problem

In this section we provide details of the algorithmic procedure adopted for solving the inverse problem, i.e. reconstructing the distribution $P(\tilde{k})$ from Eq. (12). In the HMF formulation, the field $Y(t)$ is generated by an infinite number of neurons and \tilde{k} is a continuous variable in the interval $[0, 1]$. In practice, we can sample uniformly this unit interval by L disjoint subintervals of length $1/L$, labelled by the integer i . This corresponds to an *effective neural index* i , that identifies the class of neurons with in-degree $\tilde{k}_i = i/L$. In this way we obtain a discretized definition converging to Eq.(12) for $L \rightarrow \infty$:

$$Y(t) = \int_0^1 P(\tilde{k}) y_{\tilde{k}}(t) d\tilde{k} \simeq \frac{1}{L} \sum_{i=0}^{L-1} P(\tilde{k}_i) y_{\tilde{k}_i}(t). \quad (17)$$

In order to improve the stability and the convergence of the algorithm by smoothing the fluctuations of the fields $y_{\tilde{k}_i}(t)$, it is convenient to consider a coarse-graining of the sampling by approximating $Y(t)$ as follows

$$Y(t) = \frac{1}{L'} \sum_{i=0}^{L'-1} P(\tilde{k}_i) \langle y_{\tilde{k}_i}(t) \rangle. \quad (18)$$

where $\langle y_{\tilde{k}_i}(t) \rangle$ is the average of L/L' synaptic fields of connectivity $\tilde{k} \in [\tilde{k}_i, \tilde{k}_{i+1}]$. This is the discretized Fredholm equation that one can solve to obtain $P(\tilde{k}_i)$ from the knowledge of $\langle y_{\tilde{k}_i}(t) \rangle$ and $Y(t)$. For this aim we use a Monte Carlo (MC) minimization procedure, by introducing at each MC step, n , a trial solution, $P_n(\tilde{k}_i)$, in the form of a normalized non-negative in-degree distribution. Then, we evaluate the field $Y_n(t)$ and the distance γ_n de-

fined as:

$$Y_n(t, P_n(\tilde{k}_i)) = \frac{1}{L'} \sum_{i=0}^{L'-1} P_n(\tilde{k}_i) \langle y_{\tilde{k}_i}(t) \rangle \quad (19)$$

$$\gamma_n(P_n(\tilde{k}_i))^2 = \frac{1}{t_2 - t_1} \int_{t_1}^{t_2} \frac{[Y_n(t, P_n(\tilde{k}_i)) - Y(t)]^2}{Y^2(t)} dt. \quad (20)$$

The time interval $[t_1, t_2]$ has to be taken large enough to obtain a reliable estimate of γ_n . For instance, in the case shown in Fig.4, where $Y(t)$ exhibits an almost periodic evolution of period $T \approx 1$ in the adimensional units of the model, we have used $t_2 - t_1 = 10$. The overall configuration of the synaptic fields, at iteration step $n + 1$, is obtained by choosing randomly two values \tilde{k}_j and \tilde{k}_l , and by defining a new trial solution $\bar{P}_{n+1}(\tilde{k}) = P_n(\tilde{k}) + \epsilon \delta_{\tilde{k}, \tilde{k}_j} - \epsilon \delta_{\tilde{k}, \tilde{k}_l}$, so that, provided both $\bar{P}_{n+1}(\tilde{k}_j)$ and $\bar{P}_{n+1}(\tilde{k}_l)$ are non-negative, we increase and decrease $P_n(\tilde{k}_j)$ of the same amount, ϵ , in \tilde{k}_j and \tilde{k}_l respectively. A suitable choice is $\epsilon \sim \mathcal{O}(10^{-4})$. Then, we evaluate $\gamma_{n+1}(\bar{P}_{n+1}(\tilde{k}_i))$: If $\gamma_{n+1}(\bar{P}_{n+1}(\tilde{k}_i)) < \gamma_n(P_n(\tilde{k}_i))$ the step is accepted i.e. $P_{n+1} = \bar{P}_{n+1}$, otherwise $P_{n+1} = P_n$. This MC procedure amounts to the implementation of a *zero temperature dynamics*, where the cost function $\gamma_n(P_n(\tilde{k}_i))$ can only decrease. In principle, the inverse problem in the form of Eq.(18) is solved, i.e. $Y_n(t, P_n(\tilde{k}_i)) = Y(t)$, if $\gamma_n(P_n(\tilde{k}_i)) = 0$. In practice, the approximations introduced by the coarse-graining procedure do not allow for a fast convergence to the exact solution, but $P_n(\tilde{k}_i)$ can be considered a reliable reconstruction of the actual $P(\tilde{k})$ already for $\gamma_n < 10^{-2}$. We have checked that the results of the MC procedure are quite stable with respect to different choices of the initial conditions $P_0(\tilde{k}_i)$, thus confirming the robustness of the method.

We want to conclude by commenting on the very definition of the coarse-grained synaptic field $\langle y_{\tilde{k}_i}(t) \rangle$. Since small differences in the values of \tilde{k}_i reflect in small differences in the dynamics, for not too large intervals $[\tilde{k}_i, \tilde{k}_{i+1}]$ the quantity $\langle y_{\tilde{k}_i}(t) \rangle$ can be considered as an average over different initial conditions. For locked neurons the convergence of the average procedure defining $\langle y_{\tilde{k}_i}(t) \rangle$ is quite fast, since all the initial conditions tend to the stable fixed point, identified by the return map described in the previous subsection. On the other hand, the convergence of the same quantity for unlocked neurons with chaotic dynamics should require an average over a huge number of initial conditions. For this reason, the broader is the distribution, i.e. the bigger is the unlocked chaotic component (see Fig.2 of the main paper), the more computationally expensive is the solution of the inverse problem. This numerical drawback for broad distributions emerged in our tests of the inversion procedure described in Fig. 3 of the main paper. Moreover, such tests showed that the procedure works insofar the QSE are not neg-

ligible, but it fails in the absence of the locking mechanism. In this case, indeed, the global field $Y(t)$ is constant and also $\langle y_{\tilde{k}_i}(t) \rangle$ become constant, when averaging over a sufficiently large number of samples. In this situation Eq.(18) becomes trivial and cannot be used to evaluate $P(\tilde{k}_i)$. We want to observe that, while in general

$y_{\tilde{k}_i}(t) \neq \langle y_{\tilde{k}_i}(t) \rangle$, one can reasonably expect that $\langle y_{\tilde{k}_i}(t) \rangle$ is a very good approximation of $\langle y_{\tilde{k}_i}(t) \rangle$. This remark points out the conceptual importance of the HMF formulation for the possibility of solving the inverse problem.

-
- [1] Xiao Fan Wang, Int. J. Bifurcation Chaos, 12, 885 (2002).
 - [2] A. Barrat, M. Barthélemy, and A. Vespignani, *Dynamical Processes on Complex Networks*, Cambridge University Press, Cambridge, UK (2008).
 - [3] S. N. Dorogovtsev, A.V. Goltsev, and J. F. F. Mendes, Rev. Mod. Phys. 80, 1275 (2008).
 - [4] R. Cohen, S. Havlin, *Complex Networks: Structure, Robustness and Function*, Cambridge University Press, Cambridge, UK, 2010.
 - [5] A. Arenas, A. Daz-Guilera, J. Kurths, Y. Moreno, C. Zhou, Phys. Rep. 469, 93 (2008).
 - [6] S. Boccaletti, V. Latorab, Y. Morenod, M. Chavez, D.-U. Hwanga, Phys. Rep. 424, 175 (2006).
 - [7] L. Donetti, P. I. Hurtado, and M. A. Muñoz, Phys. Rev. Lett. 95, 188701 (2005).
 - [8] E. Schneidman, M. J. Berry, R. Segev, and W. Bialek, Nature 440, 1007 (2006); S. Cocco, S. Leibler, R. Monas-son, Proc. Natl. Acad. Sci. U.S.A. 106 14058 (2009).
 - [9] S. G. Shandilya and M. Timme, New J. Phys. 13 013004 (2011).
 - [10] Hong-Li Zeng, Mikko Alava, Erik Aurell, John Hertz, and Yasser Roudi, Phys. Rev. Lett. 110, 210601 (2013).
 - [11] E. Niedermeyer, F. H. Lopes da Silva, *Electroencephalography: Basic Principles, Clinical Applications, and Related Fields*, Lippincott Williams & Wilkins, (2005).
 - [12] S.A. Huettel, A.W Song & G. McCarthy *Functional Mag-
netic Resonance Imaging*, Sunderland, MA: Sinauer As-
sociates, (2009).
 - [13] M. Tsodyks and H. Markram, Proc. Natl. Acad. Sci. USA 94, 719 (1997).
 - [14] M. Tsodyks, K. Pawelzik and H. Markram, Neural Comput. 10, 821, (1998).
 - [15] R. Kress, *Linear Integral equations* Applied numerical sciences, v.82, Springer-Verlag, New York, (1999).
 - [16] M. Tsodyks, A. Uziel and H. Markram, The Journal of Neuroscience 20, RC1 (1-5) (2000).
 - [17] V. Volman, I. Baruchi, E. Persi and E. Ben-Jacob, Physica A 335, 249 (2004).
 - [18] M. di Volo and R. Livi, J. of Chaos Solitons and Fractals 57, 54–61 (2013).
 - [19] M. di Volo, R. Livi, S. Luccioli, A. Politi and A. Torcini, Phys. Rev. E 87, 032801 (2013).
 - [20] F. Chung, Linyuan Lu: *Complex Graphs and Networks*, CBMS Series in Mathematics, AMS (2004).
 - [21] R. Brette, Neural Comput. 18, 2004 (2006).
 - [22] R. Zillmer, R. Livi, A. Politi, and A. Torcini, Phys. Rev. E 76, 046102 (2007).
 - [23] Supplementary Materials
 - [24] M. Tsodyks, I. Mitkov, and H. Sompolinsky, Phys. Rev. Lett. 71, 1280 (1993).